Hidden phases in homovalent and heterovalent substituted BaTiO₃

Florian Mayer [*], Marco Deluca, and Maxim N. Popov [†]

Materials Center Leoben Forschung GmbH, Roseggerstrasse 12, 8700 Leoben, Austria

Ferroelectric materials can exhibit metastable phases when exposed to THz pulses, characterized by a polarization integration capability related to the amplitude and frequency of the pulses. These so-called "hidden" phases enable gradual switching of polarization that can be utilized in artificial synapses for nonconventional (neuromorphic) computing machines. In this work, we employ large-scale molecular-dynamics simulation based on an effective Hamiltonian approach, and we report on the discovery of hidden phases in Zr- and Nb-doped barium titanate (BaTiO₃). We investigate the formation and the stability of those phases at different stimuli and temperatures (20 and 200 K). Our results shed light on the compositional dependence of the properties of these phases, demonstrating the potential of lead-free relaxor ferroelectrics for near-room-temperature neuromorphic computing.

I. INTRODUCTON

Artificial intelligence is almost indispensable today, and a great deal of effort is being put into developing new and better computing techniques compared to the traditional Von Neumann architecture. A subarea of this research is the so-called neuromorphic computing, which is a rapidly growing interdisciplinary research field [1]. Within this concept, an attempt is made to mimic the characteristics and functionalities of neurons and their networks, such as memory, learning, and massive parallelism, via software and novel hardware. For the latter, the development and discovery of new materials or the tuning of properties of existing materials is inevitable. A class of materials showing promising properties for this purpose are ferroelectric materials and substituted versions thereof [2]. In this context, the out-of-equilibrium long-lived phases of matter appearing upon THz-irradiation recently reported in relaxor ferroelectrics Pb(Mg₁/₃Nb₂/₃)O₃ (PMN) [3] and Pb(Zr, Ti)O₃ (PZT) [4], as well as in antiferroelectric NaNbO₃ [5], offer intriguing prospects. These phases are often referred to as "hidden phases", due to their metastable nature and inaccessibility under equilibrium conditions. The presence of hidden phases results in a gradual switching of the electric polarization when the THz pulses are applied with a high repetition rate. Moreover, the polarization states persist even after removal of the external stimuli. Both of these properties—gradual (analog) switching and nonvolatility—are sought after for mimicking synaptic behavior in artificial synapses. Gradual switching of the remanent polarization in ferroelectrics has also been experimentally demonstrated in, e.g., PZT [6], however it happens at a much slower pace. Also, applying strain *nanosecond* pulses has been shown to result in a gradual switching in PZT [7]. Hence, quasianalog switching between hidden phases

happening at a picosecond timescale combined with their persistence offers an attractive playground for applications in ultrafast neuromorphic, i.e., brain-inspired, computing. Such materials can be potentially used in ferroelectric tunnel junctions (FTJ) to modulate tunneling currents via the tunneling electroresistance (TER) effect [8], i.e., in resistors with memory (memristors). Alternatively, one can also create capacitors with memory (memcapacitors), which can result in even more energy-efficient neuromorphic devices [9]. In previous works [3–5], either pure substances (NaNbO₃) or solid solutions with a fixed composition (PMN and PZT) were considered. That is, the effect of varying the composition of such a solid solution has so far remained unexplored. In this work, we present *ab initio*–based simulations leading to the discovery of hidden phases in lead-free relaxor Zr- and Nb-doped BaTiO₃ (BT) solid solutions [BaZr$_x$Ti$_{1-x}$O₃ (BZT) and BaNb$_x$Ti$_{1-x}$O₃ (BNT)], we characterize their behavior under applied THz pulses, explore compositional tuning of the gradual polarization switching, and discuss possible implications for designing synaptic devices based on the hidden phases.

The paper is organized as follows: In Sec. II, the theoretical foundations of the simulations used are explained by means of so-called effective Hamiltonians. This is followed by a detailed analysis of the results in Sec. III, where several important quantities are discussed. This includes a study of hidden phases in the respective systems as well as the gradual switching of the electric polarization. Subsequently, the stability and reversibility of the induced phases are also examined. Finally, a study at higher temperatures is discussed, and stability problems are explained.

II. METHODOLOGICAL DETAILS

A. Effective Hamiltonian

All simulations in this work are based on the concept of effective Hamiltonians [10–14], which are used to describe the potential energy surface of the considered systems. The main difference from other potentials used in molecular-dynamics

*florian.mayer@mcl.at
†maxim.popov@mcl.at

(MD) simulations is the choice of the parametrization basis. Instead of considering the atoms individually, in an effective Hamiltonian the description of the energy is based on a basis of phonon modes [10]. Therefore, the amplitudes [11] of selected phonon modes serve as central variables, with amplitude vectors defined for each unit cell in a given supercell. Additionally, a dimensionless displacement vector [11] is defined for each unit cell to account for inhomogeneous strains. The homogeneous strain is taken into account via using the deformation of the whole supercell [11,12]. A detailed description of the formalism can be found in Refs. [11–13]. In general, the effective Hamiltonian consists of the following energy contributions: Local-mode self-energy, homogeneous and inhomogeneous contributions to the elastic energy, dipole-dipole interaction, short-range interactions, strain-phonon coupling, and interactions with an external field. The parametrization of the required parameters can be done entirely by using first-principles calculations [15]. The effective Hamiltonian formalism, originally derived only for pure systems, has been recently extended in order to be able to describe substituted systems [16–19]. The incorporation of substituted atoms can be done in different ways. For the parametrization of the base system, either (i) the virtual crystal approximation [16,20] (VCA) can be used, (ii) the two systems can be simply averaged [21], or (iii) one of the two systems can be defined as the parent system [18]. The effects caused by substitution are further taken into account by additional terms in the Hamiltonian. This allows us to account for different local-mode self-energies, different long-range interactions, and the influence of substitution atoms on neighboring unit cells. In this work, we use the approach from Ref. [22], which considers the substituted atoms as a perturbation of the pure system. The associated Hamiltonian for pure BT was parametrized using a significant number of anharmonic couplings to higher-energy phonons, leading to an improved description of the transition temperatures of pure BT [13]. Furthermore, the inclusion of Zr^{4+} and Nb^{5+} was performed by using additional terms to the Hamiltonian, showing excellent agreement of the simulated phase diagrams with experimental data [22]. It should be noted that the effective Hamiltonian for BNT includes the treatment of Ti vacancies as the main charge compensation scheme in this material [23]. All required parameters for the extended effective Hamiltonian are listed in the Supplemental Material of Ref. [22].

B. Molecular dynamics

To simulate properties at finite temperatures, we use MD simulations. The fundamental basis of these simulations is the potential energy surfaces in the form of effective Hamiltonians as described in the previous section. To make use of the effective Hamiltonian formalism in terms of MD simulations, we use the FERAM code developed by Nishimatsu and co-workers [11,12,21]. This code was adapted in order to take into account the additional terms from Ref. [22]. In addition, a function was added to be able to apply customized external fields during our simulations. Since we want to compare our materials of interest with simulations from the literature, we decided to apply the same external stimuli as in Refs. [3,5].

The corresponding formula of the applied external field is defined in Eq. (1). Here, E_0 denotes the amplitude of the pulse, t_0 is the position of the maximum, t is the time variable, w represents the angular frequency, and Δ is the width of the Gaussian function. The parameters are also taken from Ref. [3] and read $E_0 = 4\sqrt{3} \times 10^7$ V/m, $\Delta = 0.2$ ps, and $\omega/2\pi = 1.5$ THz. For all simulations, the field was applied along the $\langle 111 \rangle$ direction,

$$\boldsymbol{E}_{\text{ext}}(t) = \boldsymbol{E}_0 e^{-\frac{(t-t_0)^2}{\Delta^2}} \cos(\omega(t - t_0)). \tag{1}$$

The choice of parameters by Prosandeev *et al.* [3] was considered to mimic experimentally observed THz pulses [24,25]. Due to the low computational costs of effective Hamiltonian simulations, we decided to use supercells of size $96 \times 96 \times 96$ for all our investigations. Moreover, such large supercells allow better statistical quantities to be taken from the simulations. All simulations were performed using the canonical ensemble. Furthermore, a discrete time step of 2 fs was used. A velocity scaling algorithm was applied to keep the temperature constant during the simulation. To start with systems in equilibrium, each supercell was thermalized for 200 ps before applying external fields.

III. RESULTS AND DISCUSSION

A. Integration and hidden phases

Hidden phases exhibit gradual switching of polarization when a train of THz pulses is applied, referred to as "integration." In this section, we aim to study the presence of hidden phases and the integration over time for different concentrations of Zr and Nb substituted BT (i.e., BZT and BNT, respectively) by applying trains of THz pulses. The shape of the pulses and its parameters have already been described in Sec. II B. As a starting point for these simulations, supercells of size $96 \times 96 \times 96$ were constructed using random distributions of substituents for both systems. It should be noted that for BNT also the right amount of Ti vacancies was included to achieve charge neutrality of the system, due to substitution with a donor cation, Nb^{5+}, occupying the atomic site of Ti^{4+}. For BZT this is not necessary since Zr^{4+} is a homovalent substituent for Ti^{4+}. Following, these supercells were used to perform MD simulations at a temperature of 20 K. Later in this work, the simulation of higher temperatures is also addressed. Another important aspect for the upcoming MD simulations is the initial position of the local dipoles. Here, we decided to use two different approaches. First, we employed a starting configuration with randomly oriented dipoles, which led to a multidomain structure after thermalization for BT. For higher concentrations of substituents, states with nearly zero net polarization were observed, which are to be anticipated in such systems [22]. In the second approach, we used a ferroelectric single-domain distribution of dipoles as a starting point. This approach led for small concentrations to a preservation of this state, whereas for higher concentrations the thermalization was not sufficient to move from this state to a state of vanishing polarization typically observed in that concentration range [22]. As we are primarily interested in identifying the compositions with the best properties for integration, stability, and reversibility, results for both starting
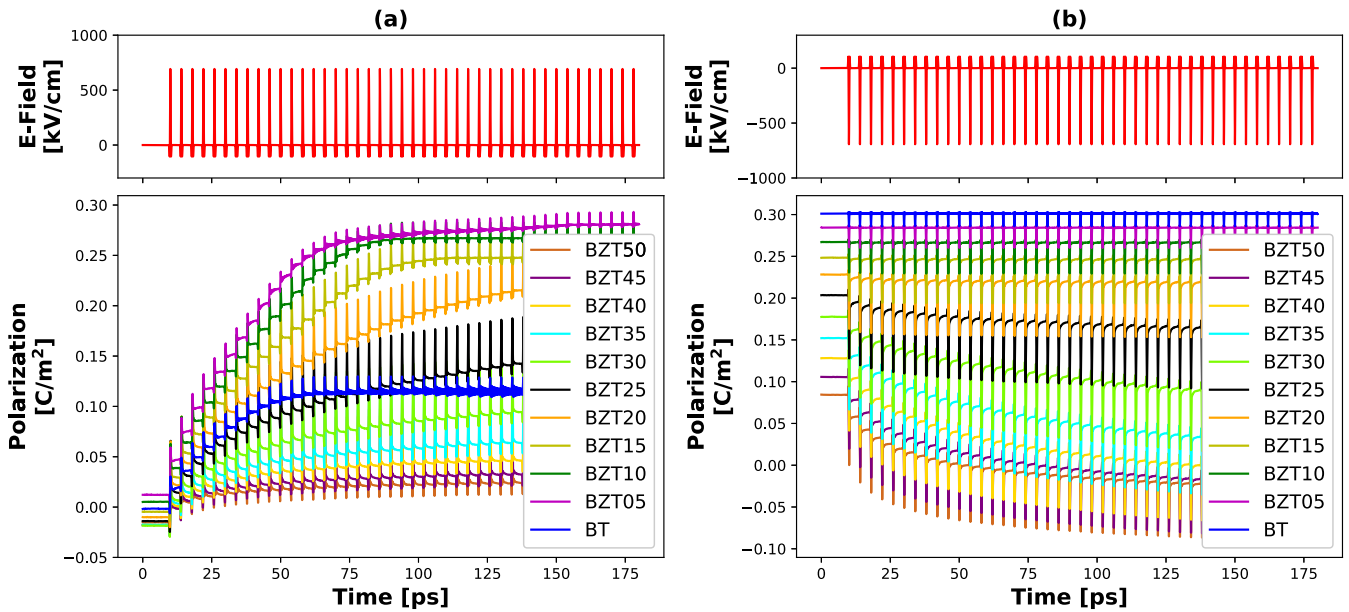
FIG. 1. Evolution of polarization in BZT (from 0% to 50% Zr content) due to an applied train of THz pulses (at 20 K). The polarization refers to the z-component of the averaged supercell polarization. Part (a) shows the results starting from a random configuration, and (b) illustrates the results starting from a single-domain configuration. The system was equilibrated for 200 ps before the first trends were plotted.

conditions are shown in the course of this section. This allows us to better understand the occurrence of hidden phases and to investigate their basic mechanisms.

To start with our investigation, we first want to focus on the case of BZT where the corresponding results are presented in Fig. 1. Figure 1(a) illustrates the results for a starting configuration of randomly distributed dipoles, where a train of pulses with positive polarity was applied after thermalization. In Fig. 1(b), a single-domain configuration was chosen as the starting configuration, with a negative-polarity pulse train applied after thermalization. The results of Fig. 1(a) shall be discussed first. Here, after thermalization, a nearly vanishing polarization is observed for all compositions studied. For the case of small concentrations, a multidomain configuration of the dipoles is observed. This is confirmed by the illustration of the dipole pattern for the case of pure BT and BZT05 (i.e., 5% of Zr) in Fig. 2. In this figure, snapshots for different compositions are presented at three different times during the simulations. The first snapshot was taken right after thermalization, the second one at 40 ps, and the third one at 180 ps after thermalization. For higher concentrations, a nearly vanishing net polarization is found in Fig. 1(a), which is to be expected for these systems [22]. Applying a positive train of pulses now has the following effects on the polarization states: For BT, an integration (i.e., a gradual increase of polarization induced by the train of pulses) of the polarization is observed, with the saturation polarization lying in the middle range compared to the other compositions. The reason that BT does not exhibit the largest net polarization of all compositions can again be found in Fig. 2. Here, it is clear that the train of pulses can change the orientation of parts of the multidomain configuration but not reach a pure single-domain state. That is, the applied pulses are simply not strong enough, and a larger amplitude has to be applied to reach the single-domain state. Furthermore, in Fig. 1(a), a small amount of 5% Zr

already changes the observed integration of the polarization significantly. In contrast to pure BT, the saturation polarization is almost twice as large. This can be explained by the partial disruption of the long-range correlation of the dipoles induced by the impurity ions, leading to higher fragmentation of the polar order. This facilitates reaching a near-perfect single-domain state as demonstrated by the case of BZT05 in Fig. 2 at 180 ps. If the concentration is increased further, the saturation polarization decreases, which is to be expected in such a system. This is caused by the nonpolar nature of the unit cells centered on Zr impurity cations, which reduces the overall polarization. Furthermore, for higher concentrations, the long-range correlation of the dipoles is further and further disrupted until the systems are in a state where only a mixture of equally sized polar and nonpolar nanodomains is present. The occurrence and behavior of such nanodomains is confirmed in Fig. 2 with the example of BZT35. The appearance of nanodomains is consistent with the concentration range where relaxor behavior is also observed. Based on the results from Fig. 1(a), two main differences can be identified for the integration of polarization as well as the intermediate states. For low concentrations and BT, starting from a multidomain configuration, the ferroelectric domains are changed in size and orientation by applying the train of pulses. The intermediate states obtained are merely a different arrangement of ferroelectric domains. For larger concentrations, the disorder of the system results in an arrangement of nanodomains that are uncorrelated in the initial state. By applying the train of pulses, these nanodomains can be aligned and thus result in the measured integration of the polarization. The intermediate states are now an ensemble of correlated and uncorrelated polarization states and are further referred to as hidden phases.

As a next step, we want to discuss the results from Fig. 1(b) where the thermalization was started with a single-domain configuration. Here, it is clear that all systems show larger
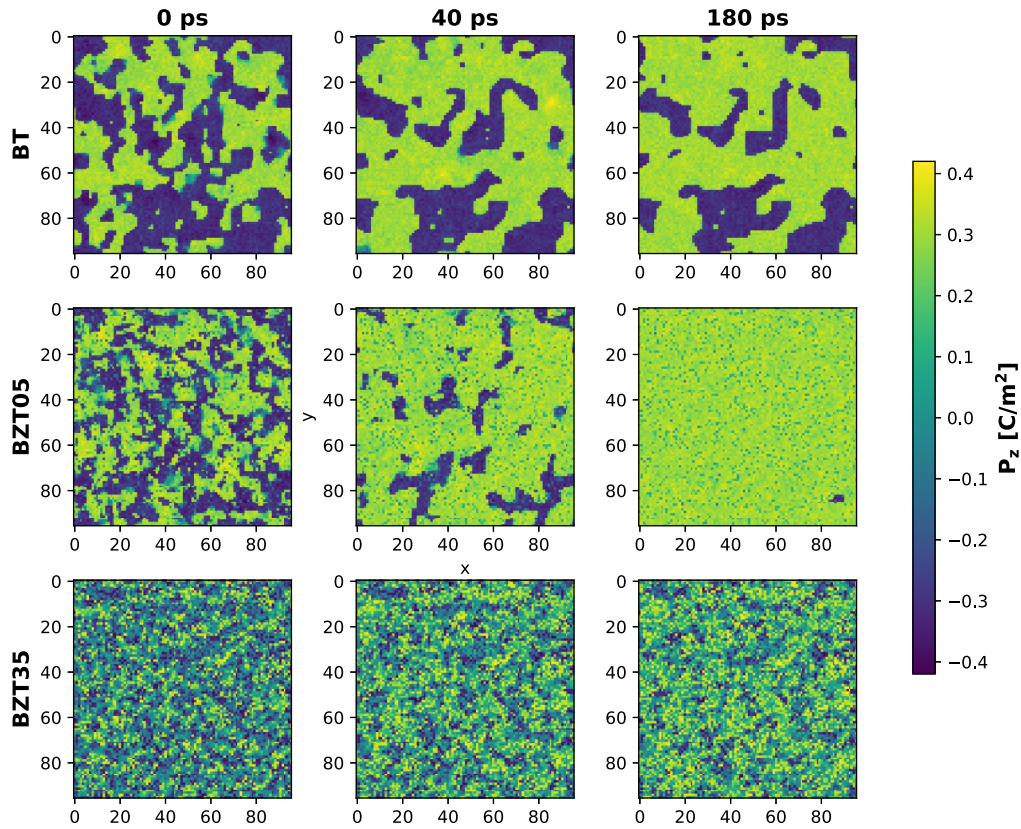
FIG. 2. Snapshots of the compositions BT, BZT05 (5% Zr), and BZT35 (35% Zr) at different times of the simulation (at 20 K). The color represents the z-component of the polarization in an $x-y$ plane of the $96 \times 96 \times 96$ supercells. The 0 ps snapshot was taken right after thermalizing the system for 200 ps.

net polarization after thermalization compared to Fig. 1(a). That is, for BT and small concentrations, the systems are in a pure single-domain state. For higher concentrations, the nanodomains are correlated and no vanishing polarization state is established. For all compositions, therefore, it can be seen that such an induced state is certainly stable in the simulation, and that thermalization has not caused any major relaxations either. Furthermore, it can be observed how the net polarization decreases with increasing Zr content. For more details on this decrease of polarization, we refer to the Supplemental Material [26]. In the following, we will investigate how the individual systems behave when the same train of pulses from before is applied but only inverted. For BT and concentrations lower than 25%, no significant change of the polarization can be achieved by applying the train of pulses. This shows that once the system is in such a single-domain configuration, the selected pulse shape can no longer break it up. In this case, the pulses would have to be significantly higher in order to achieve changes. We shall stress that switching behavior is dependent on the parameters of the external stimulus. For instance, domain-wall motion has been reported for a similar magnitude of the E-field, but a longer pulse width (up to ns) in BaTiO$_3$ [27]. If the concentration is now increased, the ferroelectric domains become smaller and smaller down to nanodomains. These nanodomains are also in this case initially aligned and correlated similar to a single domain, but the pulses gradually manage to align them differently and thus to change the overall polarization. In principle, such negative

integration starting from a saturated state is the reversibility of the induced polarization, which is discussed in detail in Sec. III C. In summary, the following statements can be drawn for integration in BZT: If a multidomain configuration is taken as the starting point, integration to the highest saturated polarizations is seen at rather low concentrations of Zr. For BT, on the other hand, the selected pulse is not sufficient to align all ferroelectric domains. However, for both cases, no negative integration is observed at unchanged pulses, which can be attributed to the strong correlation between the individual local dipoles. At higher concentrations, the reached saturated polarization becomes lower, but integration is also possible in the other direction. This is caused by the diversity of hidden phases and the rather simple alignment of the nanodomains by the selected train of pulses. In general, compositions with concentrations above 25% Zr provide a better basis for application to mimic synapses when considering the chosen shape of the applied train of pulses and the respective integration in both directions.

As a further step, we will conduct an analogous study for the case of BNT, with the results of the simulations displayed in Fig. 3. The two different starting conditions were also included in this study, with the results in Fig. 3(a) obtained from the random input configuration discussed first. The results for pure BT have already been discussed in detail and will therefore not be discussed again. Concerning the substituted systems, the trend for BNT is quite similar to that of BZT, but there are differences in the concentration range as well
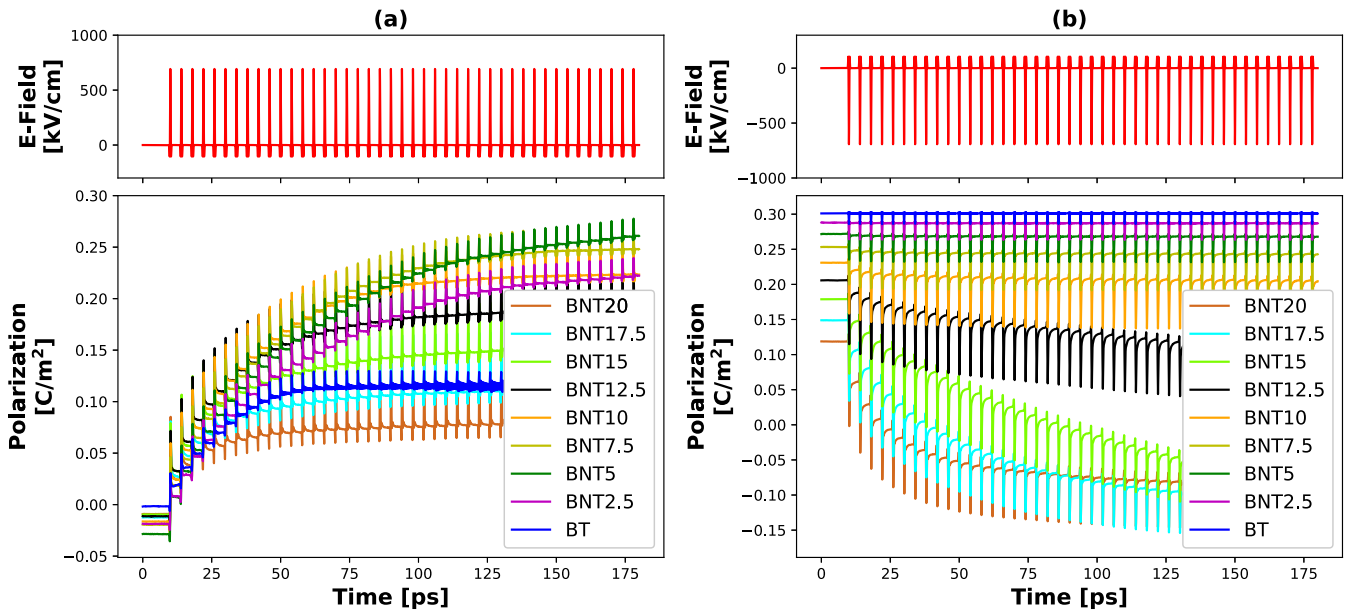
FIG. 3. Evolution of polarization in BNT (from 0% to 20% Nb content) due to an applied train of THz pulses (at 20 K). The polarization refers to the z-component of the averaged supercell polarization. Part (a) shows the results starting from a random configuration, and (b) illustrates the results starting from a single-domain configuration. The system was equilibrated for 200 ps before the first trends were plotted.

as the achieved saturated polarizations. As in the case of BZT, an increase in saturated polarization is found for small concentrations compared to pure BT. This is again due to the partial disruption of the long-range interaction by substituents, thereby facilitating the alignment of the ferroelectric domains by the train of pulses. Furthermore, this behavior can be illustrated also in BNT by plotting snapshots from the simulations as shown in Fig. 4. Here, significantly smaller ferroelectric domains are observed for BNT05 compared to BT right after thermalization. In addition, also the integration up to a nearly single-domain state at 180 ps is evident. If the concentration is increased further, the saturated polarization decreases again. This behavior is again comparable with BZT, but here the saturation polarization decreases faster at the same concentration, which is compatible with the evolution of relaxor behavior in heterovalent substituted BaTiO$_3$ systems [23]. For the case of BNT15, after thermalization, noncorrelated nanodomains result. The corresponding polar structure can be found in Fig. 4. If the train of pulses is applied for this system, the nanodomains can align and result in a variety of different possible intermediate states, which again can be referred to as hidden phases. In this case, a distinction must also be made between small and larger concentrations. For smaller concentrations, the intermediate states are merely a variety of different ferroelectric domains with different sizes and orientations. For larger concentrations from about 10% of Nb, the ferroelectric order is destroyed to such an extent that one can only speak of nanodomains (i.e., similar to what happened in BZT with 25% of Zr and above). The occurrence of such nanodomains coincides with the concentration range where relaxor behavior is also observed.

In the following, we will now investigate how the compositions behave when a single-domain state is used as starting configuration. The corresponding results are shown in Fig. 3(b). Here, again, an increased polarization state is

obtained for all systems after thermalization. For smaller concentrations, the induced single-domain state remains. But even for larger concentrations, no major relaxations to a vanishing polarization are observed. That means that, in this case, nanodomains remain also correlated after thermalization and provide a polarization state that differs from the single-domain state by the reduced net polarization. If the inverted pulse train is now applied, the following observations can be made: For concentrations lower than 7.5%, there is no significant change in the net polarization, and the systems remain in their initial state. The correlation between the local dipoles is so strong here that no repolarization of the system can be induced by the selected shape of the train of pulses. However, at concentrations higher than 7.5%, the sizes of the ferroelectric domains already become so small that other polarization states can be introduced by applying a negative train of pulses. The higher the concentration becomes, the easier it is for the selected pulse to break the correlation and align the nanodomains differently. This behavior is analogous to BZT, but the concentration range for the occurrence of negative integration is much smaller here starting at about 10% of Nb, whereas in BZT more than 25% of Zr was necessary to induce the same effect. This is again in accord with the evolution of relaxor behavior in heterovalent substituted BT [23]. Considering the selected pulse, the interesting concentration range is also specified here with concentrations above 10% for the application to mimic synapses. However, it should be emphasized that these results depend on the selected shape of the pulse and that the concentration ranges listed are only indicative values for the upcoming further analyses.

B. Stability

Here, we examine the stability of the hidden phases over a certain period of time. This is done by means of the MD
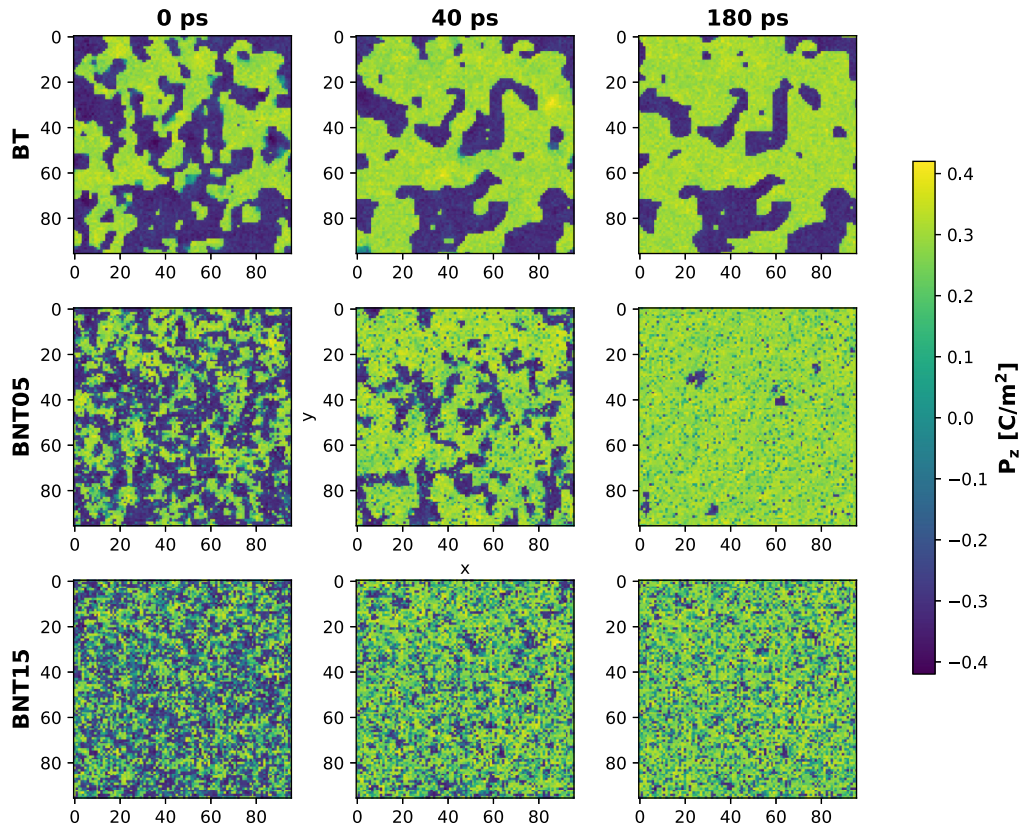
FIG. 4. Snapshots of the compositions BT, BNT05 (5% Nb), and BNT15 (15% Nb) at different times of the simulation (at 20 K). The color represents the z-component of the polarization in an $x-y$ plane of the $96 \times 96 \times 96$ supercells. The 0 ps snapshot was taken right after thermalizing the system for 200 ps.

simulations, where a different number of pulses are applied to induce the individual states. Furthermore, the simulations for the individual states are continued without external stimuli, and their evolution is monitored. It should be mentioned that the simulations can only run for a limited time due to resource constraints and thus the stability can only be ascertained for this time range. We thermalized the individual simulations first for 200 ps and then ran them for another 180 ps. To reduce computational load, we tested stability only for selected compositions of BZT and BNT, based on the insight from the previous sections. Specifically, we decided to use the BZT35 (35% Zr) and BNT15 (15% Nb) compositions due to the favorable integration properties and both systems being in the concentration range where relaxor behavior is observed. First, the BZT35 composition is investigated in more detail, with the associated results presented in Fig. 5(a). Here, the system was thermalized and subsequently the excitation of the system was started by applying 1–15 pulses. After applying each group of pulses, the simulation was continued over several decades of picoseconds. It can clearly be seen that various intermediate polarization states are reached. The spacing between these states varies and becomes smaller with each next pulse, as illustrated in the inset of Fig. 5(a). For the temperature of 20 K, the obtained states appear rather stable over the simulated time period, similar to PMN [3]. However, if the polarization curves are examined more closely, a tendency to creep towards lower polarizations becomes apparent, which can be clearly

seen in Fig. 6(a). This creep indicates that BZT35 strives for an equilibrium state with significantly lower polarization. This tendency is consistent with the expected zero net polarization state in a relaxor ferroelectric [22]. All in all, the induced states can be considered to be metastable over a time range of several decades of picoseconds. To study stability on longer timescales, the simulations would have to be extended considerably, but this is not feasible even with the low-cost effective Hamiltonians. The number of states that can still be distinguished from each other also plays an important role for the application. In the case of BZT35, multiple states can be clearly separated. However, if the polarization approaches saturated polarization, the states become blurred and can only be hardly distinguished.

An analogous study is now presented for the BNT15 composition. The protocol for the MD simulations is the same as that already explained in detail for BZT35. The corresponding results can be seen in Fig. 5(b). At first glance, a significant number of induced states can also be seen here, whereby these states also appear stable over the simulated time span. A more detailed analysis also shows a creep of the individual states. It is observed that after excitation the individual states slowly creep to lower polarizations, as evident in Fig. 6(b). This creep is again expected for the BNT15 system, since the ground state of this relaxor ferroelectric is associated with vanishing polarization. However, this creep is barely noticeable over the simulated time period. The number of clearly distinguishable
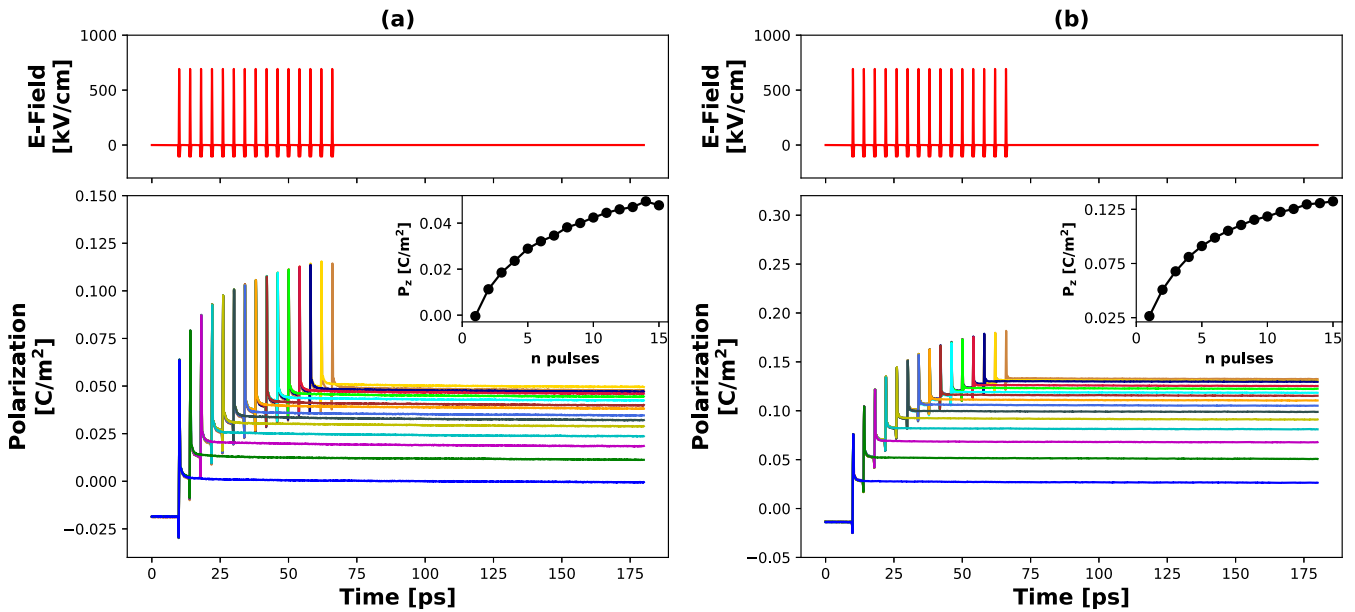
FIG. 5. Stability of hidden phases at 20 K obtained from MD simulations. Part (a) shows the stability for BZT35 (35% Zr), and (b) illustrates the stability for BNT15 (15% Nb). Colors denote different number of pulses applied (blue = 1 pulse, gold = 15 pulses). The insets show the induced polarization as a function of the number of applied pulses.

states in this case is similar to BZT35, and multiple well-defined intermediate polarization states are visible. In comparison, the saturated polarization reached is more than twice as high as in BZT35. Near the saturated polarization, these states again become increasingly blurred, as is evident in
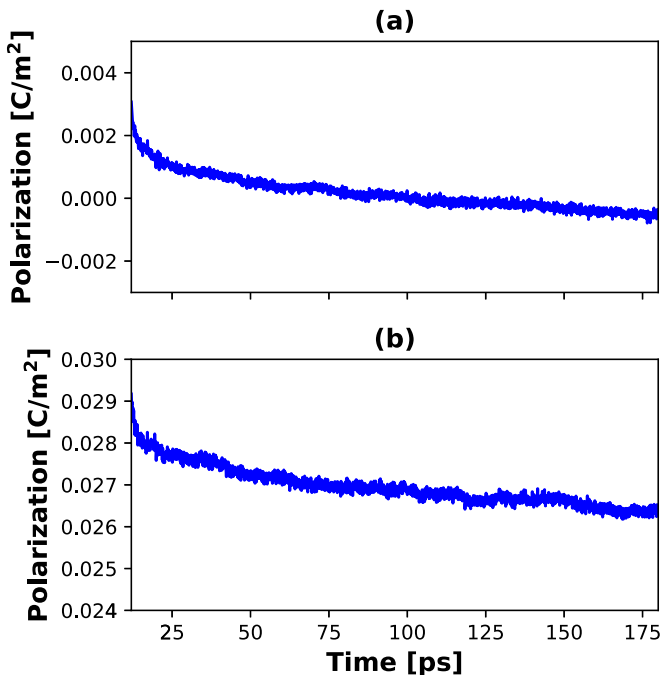

FIG. 6. Illustration of the observed creep behavior of intermediate states at 20 K. Part (a) shows the creep of the lowest induced state in BZT35 (35% Zr), and (b) demonstrates the creep of the lowest induced state in BNT15 (15% Nb).

the inset of Fig. 5(b), and it is difficult to differentiate between them.

Altogether, the stability of hidden phases can be confirmed for both systems for the simulated time span and for the selected low temperature. The number of achievable polarization states is strongly dependent on the considered composition [see Figs. 1(a) and 3(a)] and becomes smaller with increasing concentration.

C. Reversibility

Another property that is important in the possible application of such materials in neuromorphic computing devices is the possibility of reversing the induced states. To test this property, MD simulations were again employed. First, the systems were thermalized and then the application of the pulses was started. A train of pulses with positive amplitudes was first applied until integration near saturated polarization was achieved. Then, a train of pulses with negative polarity was applied to check if the integration also occurs starting from such an induced state, and brings the system to opposite polarization states. To be consistent with the previous sections, the two systems BZT35 and BNT15 are also examined here. The reversibility results for BZT35 can be found in Fig. 7(a). Here, the integration of the polarization over time is observed initially. The polarization saturates gradually up to the maximum value from Fig. 1(b). Since this saturation is rather slow, the application of positive pulses was stopped after a certain time and continued with the application of negative pulses. The negative pulses lead to a gradual decrease of the polarization, followed by the inversion of the polarization and further integration. The progression of integration after switching polarity of the pulses is slightly different compared to the integration before switching and implies that different states can be accessed here. Through this simulation, we confirm
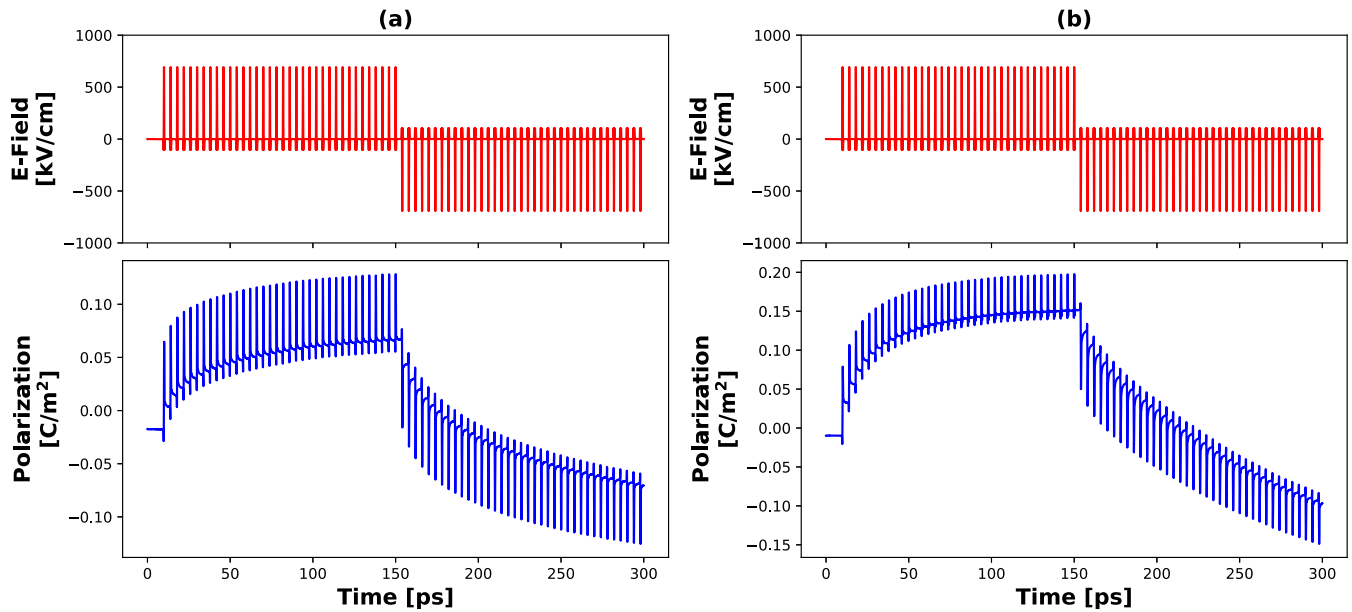
FIG. 7. Reversibility at 20 K obtained by applying a train of pulses and then inverting the amplitude. Part (a) shows the reversibility of BZT35 (35% Zr), and (b) illustrates the reversibility of BNT15 (15% Nb).

the feasibility of gradual polarization reversal in BZT35 by applying a negative train of pulses. The polarization reversal allows us to attain negative polarization values well below the initial state prior to pulse application.

The same method is used next to investigate reversibility for BNT15. The corresponding results can be seen in Fig. 7(b). Again, after thermalization of the system the simulation was started with a positive train of pulses. This results in an integration of the polarization that appears to start saturating with increasing time to a maximum polarization level as presented in Fig. 1(b). Afterwards the train of pulses was inverted and a negative integration of the polarization can be observed. The progression of this negative integration is different from the positive integration, which means that different states can be accessed. Compared to BZT35, the negative integration in BNT15 is nearly linear, showing the variety of different hidden phases and the different response to the train of THz pulses in these systems. Altogether, also for the case of BNT15, it can be confirmed by this kind of simulation that the induced polarization can be inverted using a negative train of pulses.

Further possibilities of reversibility and problems that can occur at lower concentrations of substituents will also be discussed here. As an alternative method for returning to the initial state after excitation of the system, an increase in temperature can be used [3]. Increasing the temperature results in a strong increase of the mobility of the local dipoles, and thus the induced polarization state decays. However, the required temperature increase for reversibility again depends on the considered concentrations of the respective systems. Another problem we observed at lower concentrations is that the induced polarization state is so stable that it cannot be inverted with the pulses used for excitation. This observation was also made in the work of Prosandeev *et al.* [3], although the systems considered are different. A solution to overcome this problem is again to apply a temperature increase or to

choose a larger amplitude of the negative pulse. More details on these issues and simulations of reversibility for lower concentrations can be found in the Supplemental Material [26].

D. Higher temperatures

In the previous sections, a temperature of 20 K was used to study the properties of hidden phases and their behavior. Here, we will increase the temperature to 200 K and investigate if we can observe similar results. Only results for BZT are presented here. The reason for this is that for BNT the ferroelectric phases as well as the transitions to the relaxor ferroelectric state are found at lower temperatures compared to BZT. Thus, no intermediate states can be induced at 200 K by the train of pulses because a large part of the concentration range finds itself already in the paraelectric phase at this temperature [22]. First, the integration property and the presence of hidden phases are investigated. MD simulations were performed with the same settings from Sec. III A, but the temperature was increased to 200 K. The corresponding result can be seen in Fig. 8(a). The results for pure BT and BZT05 were removed since no integration was found for these systems at 200 K. Instead of integration, these systems hopped from a multidomain configuration directly to a single-domain configuration when a single pulse was applied. For higher concentrations, integration of the polarization stimulated by the train of pulses can be observed similar to the 20 K case. Again, the integration to higher saturation polarization is found at low concentrations. The saturated polarization decreases with increasing concentration, which is consistent with the results observed in Sec. III A. However, the achievable saturated polarization for higher concentrations is much lower than previously observed. This can be attributed to the increased activity of the local dipoles, whereby the dipoles can no longer be easily stabilized into a correlated configuration. Furthermore, it is found that the peak following the excitation
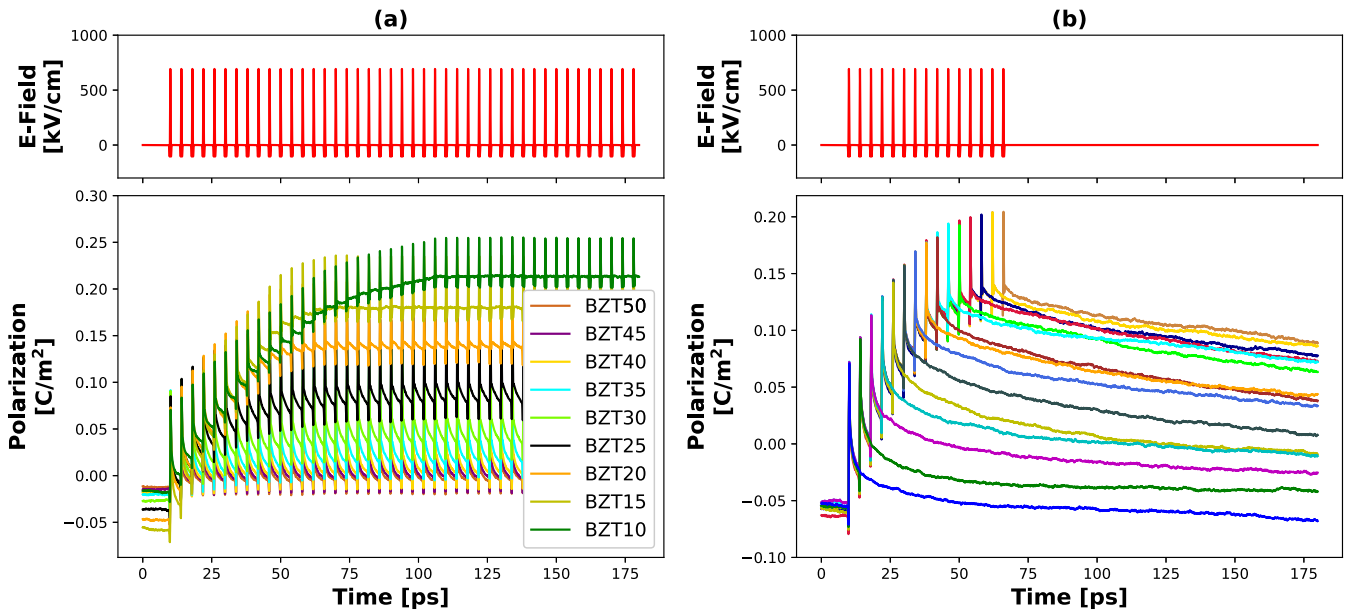
FIG. 8. Integration and stability of hidden phases in BZT at 200 K. Part (a) shows the integration of polarization when applying a train of pulses. Part (b) illustrates the stability of BZT20 (20% Zr) of hidden phases at 200 K.

is enhanced compared to the results at low temperatures. In general, an integration property is observed for BZT at a temperature of 200 K for a wide range (10–30 % Zr) of concentrations, and it can be associated with the presence of hidden phases.

The composition with 20% Zr (BZT20) was chosen here to examine the stability of the intermediate states. This concentration is slightly below the limit of relaxor behavior and shows a still reasonable number of intermediate states. The MD simulations were carried out as described in detail in Sec. III B. The corresponding results for BZT20 at a temperature of 200 K can be seen in Fig. 8(b). It can be clearly observed that different intermediate states can be achieved

by applying a different number of pulses. However, at this elevated temperature, the stability of the individual states is greatly reduced compared to the results for low temperatures. A strong relaxation to lower polarization states is observed for all intermediate states. This occurrence is expected as the system approaches a paraelectric phase with uncorrelated states at this temperature [22]. Furthermore, the increased mobility of the local dipoles counteracts the induced correlated states and aims to drive the system to an energetically lower state with lower polarization. All in all, the stability of the individual states at elevated temperature can only be confirmed for a range of several decades of picoseconds. Beyond that, the system relaxes back to a state with equilibrium polarization at a given temperature and concentration.

As a final property, the reversibility of the induced states in BZT20 is investigated. MD simulations were performed with positive and negative pulse trains, the details of which can be found in Sec. III C. The results for BZT20 at a temperature of 200 K can be seen in Fig. 9. When a positive pulse train is applied, integration of polarization is initially observed. Compared to results at lower temperature, saturated polarization is achieved faster here. Subsequently, the pulse polarity was inverted and the response of the system was investigated. The negative pulses are able to reverse the induced polarization state. Furthermore, it is found that negative integration travels through different states compared with positive integration. This shows the diversity of hidden phases in such a material.

IV. CONCLUSION

In this work, molecular-dynamics simulations based on effective Hamiltonians were used to screen Zr and Nb substituted BT (i.e., BZT and BNT, respectively) for various properties relevant to neuromorphic computing systems. The basic idea was to investigate the response of different compositions to an applied train of electric THz pulses to study the
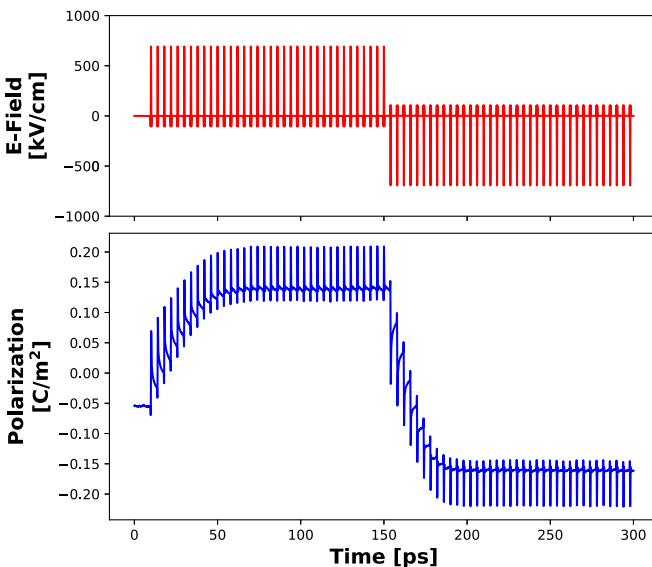

FIG. 9. Reversibility of BZT20 (20% Zr) at 200 K obtained by applying a train of pulses and then inverting the amplitude.

material's polarization integration properties, including the stability and reversibility of the achieved polarization states. For both systems, a wide range of compositions showed integration of polarization. Furthermore, the application of the external pulses revealed the presence of hidden phases, akin to those reported for PMN [3] and PZT [4]. Here, however, it must be distinguished for the respective concentration how these intermediate states appear. For small concentrations of substituent (either Zr or Nb), these intermediate states are merely differently oriented ferroelectric domains. The latter become more and more disrupted with increasing concentration of substituents (due to substituent-driven disruption of long-range ferroelectricity), leading to the appearance of polar nanodomains. The occurrence of such nanodomains was confirmed for both systems in the region corresponding to the onset of relaxor behavior. The stability of the individual intermediate states could be demonstrated for the low temperature of 20 K using the examples of BZT35 and BNT15. Here, a slight creep to lower polarization states was detected for both cases. Consequently, reversibility was also demonstrated for the examples of BZT35 and BNT15, where the induced polarization state could be reversed by applying a negative pulse train. Overall, the following conclusions can be drawn from the results at 20 K for the application in neuromorphic devices: The materials with composition close to the onset of the relaxor transition appear to offer the best tradeoff between (i) the range of the attainable polarizations, and (ii) the field strength required for switching/resetting the material. The former defines the number of polarization levels that can be used to encode information, i.e., the number of bits, whereas the latter determines the operation power. That means that for BZT a Zr content above 30% and for BNT an Nb content above 10% are promising for neuromorphic applications. In this range of relaxor behavior, on the one hand, an integra-

tion to reasonably saturated polarizations can be found, and on the other hand, the induced polarization can be inverted with the same shape of the pulses. Moreover, there is also stability of the intermediate states over at least several decades of picoseconds. The study at higher temperatures showed integration for concentrations above 10% of Zr, whereas for lower concentrations a direct transition to a single-domain configuration was found. The study of the stability of the intermediate states is given for the example of BZT20 only for a few decades of picoseconds. In contrast, reversibility of the induced polarization state is possible with the same pulse and was confirmed by the simulations. These results appear promising for the applications of these material in artificial synapses active near room temperature. In summary, this study demonstrates that both homovalent and heterovalent substituted $BaTiO_3$ show promising properties for use in neuromorphic computing systems if a compositional range in proximity to relaxor behavior is chosen. Such materials would be interesting for building artificial synaptic devices without the need of complex circuit design and processing, provided that sufficient maturity of the THz-technology is reached to allow the *in situ* application of pulses enabling the generation of hidden phases in those materials.

[1] D. V. Christensen, R. Dittmann, B. Linares-Barranco, A. Sebastian, M. Le Gallo, A. Redaelli, S. Slesazeck, T. Mikolajick, S. Spiga, S. Menzel *et al.*, Neuromorph. Comput. Eng. **2**, 022501 (2022).

[2] E. Covi, H. Mulaosmanovic, B. Max, S. Slesazeck, and T. Mikolajick, Neuromorph. Comput. Eng. **2**, 012002 (2022).

[3] S. Prosandeev, J. Grollier, D. Talbayev, B. Dkhil, and L. Bellaiche, Phys. Rev. Lett. **126**, 027602 (2021).

[4] S. Prosandeev, S. Prokhorenko, Y. Nahas, J. Grollier, D. Talbayev, B. Dkhil, and L. Bellaiche, Adv. Electron. Mater. **8**, 2200808 (2022).

[5] S. Prosandeev, S. Prokhorenko, Y. Nahas, Y. Yang, C. Xu, J. Grollier, D. Talbayev, B. Dkhil, and L. Bellaiche, Phys. Rev. B **105**, L100101 (2022).

[6] M. F. Sarott, M. D. Rossell, M. Fiebig, and M. Trassin, Nat. Commun. **13**, 3159 (2022).

[7] X. Shi, J. Wang, X. Cheng, and H. Huang, Adv. Theor. Simul. **5**, 2100345 (2022).

[8] A. Gruverman, D. Wu, H. Lu, Y. Wang, H. W. Jang, C. M. Folkman, M. Y. Zhuravlev, D. Felker, M. Rzchowski, C. B. Eom, and E. Y. Tsymbal, Nano Lett. **9**, 3539 (2009).

[9] K. U. Demasius, A. Kirschen, and S. Parkin, Nat. Electron. **4**, 748 (2021).

[10] W. Zhong, D. Vanderbilt, and K. M. Rabe, Phys. Rev. B **52**, 6301 (1995).

[11] T. Nishimatsu, U. V. Waghmare, Y. Kawazoe, and D. Vanderbilt, Phys. Rev. B **78**, 104104 (2008).

[12] T. Nishimatsu, M. Iwamoto, Y. Kawazoe, and U. V. Waghmare, Phys. Rev. B **82**, 134106 (2010).

[13] F. Mayer, M. N. Popov, D. M. Evans, S. Krohns, M. Deluca, and J. Spitaler, Phys. Rev. B **106**, 064108 (2022).

[14] A. Paul, J. Sun, J. P. Perdew, and U. V. Waghmare, Phys. Rev. B **95**, 054111 (2017).

[15] R. D. King-Smith and D. Vanderbilt, Phys. Rev. B **49**, 5828 (1994).

[16] L. Bellaiche, A. García, and D. Vanderbilt, Phys. Rev. Lett. **84**, 5427 (2000).

[17] L. Bellaiche, A. García, and D. Vanderbilt, Ferroelectrics **266**, 41 (2002).

[18] C. Mentzer, S. Lisenkov, Z. G. Fthenakis, and I. Ponomareva, Phys. Rev. B **99**, 064111 (2019).

[19] A. R. Akbarzadeh, S. Prosandeev, E. J. Walter, A. Al-Barakaty, and L. Bellaiche, Phys. Rev. Lett. **108**, 257601 (2012).

[20] L. Bellaiche and D. Vanderbilt, Phys. Rev. B **61**, 7877 (2000).

[21] T. Nishimatsu, A. Grünebohm, U. V. Waghmare, and M. Kubo, J. Phys. Soc. Jpn. **85**, 114714 (2016).

[22] F. Mayer, M. N. Popov, P. Ondrejkovic, J. Hlinka, J. Spitaler, and M. Deluca, Phys. Rev. B **106**, 224109 (2022).

[23] V. Veerapandiyan, M. N. Popov, F. Mayer, J. Spitaler, S. Svirskas, V. Kalendra, J. Lins, G. Canu, M. T. Buscaglia, M. Pasciak, J. Banys, P. B. Groszewicz, V. Buscaglia, J. Hlinka, and M. Deluca, Adv. Electron. Mater. **8**, 2100812 (2022).

[24] S. Lin, S. Yu, and D. Talbayev, Phys. Rev. Appl. **10**, 044007 (2018).

[25] H. Hirori, A. Doi, F. Blanchard, and K. Tanaka, Appl. Phys. Lett. **98**, 091106 (2011).

[26] See Supplemental Material at http://link.aps.org/supplemental/10.1103/PhysRevB.107.184307 for further simulations on stability, reversibility, and saturated polarization.

[27] R. Khachaturyan, A. Dimou, and A. Grünebohm, Phys. Status Solidi—Rapid Res. Lett. **16**, 2200038 (2022).